Available online at [www.sciencedirect.com](http://www.sciencedirect.com)**ScienceDirect**[www.elsevier.com/locate/jes](http://www.elsevier.com/locate/jes)

**JES**  
JOURNAL OF  
ENVIRONMENTAL  
SCIENCES  
[www.jesc.ac.cn](http://www.jesc.ac.cn)

# Investigation of suitable precursors for manganese oxide catalysts in ethyl acetate oxidation

Yan Zhang<sup>1,2</sup>, Meng Wang<sup>1</sup>, Shunyu Kang<sup>1</sup>, Tingting Pan<sup>1</sup>, Hua Deng<sup>1,\*</sup>,  
Wenpo Shan<sup>1,2</sup>, Hong He<sup>1,3</sup>

<sup>1</sup>Center for Excellence in Regional Atmospheric Environment and Key Laboratory of Urban Pollutant Conversion, Institute of Urban Environment, Chinese Academy of Sciences, Xiamen 361021, China

<sup>2</sup>Zhejiang Key Laboratory of Urban Environmental Processes and Pollution Control, Ningbo Urban Environment Observation and Research Station, Chinese Academy of Sciences, Ningbo 315800, China

<sup>3</sup>State Key Joint Laboratory of Environment Simulation and Pollution Control, Research Center for Eco-Environmental Sciences, Chinese Academy of Sciences, Beijing 100085, China

---

## ARTICLE INFO

### Article history:

Received 24 August 2020

Revised 1 November 2020

Accepted 1 November 2020

---

### Keywords:

Ethyl acetate

Catalytic oxidation

Manganese

Precursor

Lattice oxygen species

---

## ABSTRACT

The control of ethyl acetate emissions from fermentation and extraction processes in the pharmaceutical industry is of great importance to the environment. We have developed three Mn<sub>2</sub>O<sub>3</sub> catalysts by using different Mn precursors (MnCl<sub>2</sub>, Mn(CH<sub>3</sub>COO)<sub>2</sub>, MnSO<sub>4</sub>), named as Mn<sub>2</sub>O<sub>3</sub>-Cl, -Ac, -SO<sub>4</sub>. The tested catalytic activity results showed a sequence with Mn precursors as: Mn<sub>2</sub>O<sub>3</sub>-Cl > Mn<sub>2</sub>O<sub>3</sub>-Ac > Mn<sub>2</sub>O<sub>3</sub>-SO<sub>4</sub>. The Mn<sub>2</sub>O<sub>3</sub>-Cl catalyst reached a complete ethyl acetate conversion at 212°C (75°C lower than that of Mn<sub>2</sub>O<sub>3</sub>-SO<sub>4</sub>), and this high activity 100% could be maintained high at 212°C for at least 100 hr. The characterization data about the physical properties of catalysts did not show an obvious correlation between the structure and morphology of Mn<sub>2</sub>O<sub>3</sub> catalysts and catalytic performance, neither was the surface area the determining factor for catalytic activity in the ethyl acetate oxidation. Here we firstly found there is a close linear relationship between the catalytic activity and the amount of lattice oxygen species in the ethyl acetate oxidation, indicating that lattice oxygen species were essential for excellent catalytic activity. Through H<sub>2</sub> temperature-programmed reduction (H<sub>2</sub>-TPR) results, we found that the lowest initial reduction temperature over the Mn<sub>2</sub>O<sub>3</sub>-Cl had stronger oxygen mobility, thus more oxygen species participated in the oxidation reaction, resulting in the highest catalytic performance. With convenient preparation, high efficiency, and stability, Mn<sub>2</sub>O<sub>3</sub> prepared with MnCl<sub>2</sub> will be a promising catalyst for removing ethyl acetate in practical application.

© 2020 The Research Center for Eco-Environmental Sciences, Chinese Academy of Sciences. Published by Elsevier B.V.

---

## Introduction

Volatile organic compounds (VOCs) emitted in a great diversity of chemical and industrial processes, as an important class of air pollutants, contributing to various environmental problems (photochemical smog, haze, and so on). Among the VOCs,

---

\* Corresponding author.

E-mail: [huadeng@iue.ac.cn](mailto:huadeng@iue.ac.cn) (H. Deng).

ethyl acetate, which is used as organic chemical raw material, extracting agent, and solvent, makes up a large proportion of emissions in the pharmaceuticals industry from fermentation and extraction processes (He et al., 2012; Zhou et al., 2015). For instance, He et al. (2012) assessed the VOC emission characteristics of 8 typical pharmaceutical enterprises in Zhejiang Province. The results indicated that the 30.41% of VOC pollution was ethyl acetate in fermentation processes while the figure was 36.64% in extraction processes, revealing the necessity of removing ethyl acetate.

Catalytic combustion is recognized as an effective method for controlling VOC emissions (Everaert and Baeyens, 2004; Kim and Shim, 2010; Kamal et al., 2016). There are two main types of catalysts for VOC catalytic oxidation including precious metal-based catalysts (Fu et al., 2017; Huang et al., 2013; Ma et al., 2008; Pei et al., 2019; Wang, 2004; Wang et al., 2013) and non-noble metal oxide catalysts (Jia et al., 2020; Deng et al., 2009; Li et al., 2016; Yang et al., 2015). Precious metal catalysts are among the main candidates for the removal of VOCs. However, precious metals have limited resources and high prices, which limit their large-scale application. Transition metal oxides (such as Fe, Cu, Mn, Co) have been widely studied in the field of catalytic combustion due to their high electron mobility and variable metal ion valences (Djinovic et al., 2020; Lu et al., 2015; Spivey, 1987; Wang and Astruc, 2017; Zhang et al., 2020a).

Manganese oxide is one of most active catalysts for removing various VOCs among the transition metal oxides (Bastos et al., 2009; Guo et al., 2019; Huang et al., 2018; Jiang et al., 2019; Zhang et al., 2020b). Wang et al. (2012) evaluated the toluene removal catalytic activity of  $\alpha$ -MnO<sub>2</sub> with various morphologies, and found that rod-like  $\alpha$ -MnO<sub>2</sub> displayed the best performance and achieved 90% toluene removal at 225°C. They concluded that the superb catalytic activity of  $\alpha$ -MnO<sub>2</sub> nanorods would be attributed to the high concentration of oxygen species and good reducibility at low temperature. Chen et al. (2020a) prepared different crystal phases MnO<sub>2</sub> catalysts ( $\alpha$ -,  $\beta$ -,  $\gamma$ -, and  $\delta$ -), and tested their performance in the benzene oxidation. The  $\alpha$ - and  $\gamma$ -MnO<sub>2</sub> catalysts owed much better activity than  $\beta$ - and  $\delta$ -MnO<sub>2</sub>, resulting from the surface lattice oxygen species. For ethyl acetate oxidation, cryptomelane-type manganese oxide, prepared via the reflux approach, could completely convert the ethyl acetate into CO<sub>2</sub> at 220°C (Santos et al., 2009). In addition to MnO<sub>2</sub>, Mn<sub>2</sub>O<sub>3</sub> has also been widely used in catalytic oxidation; for example, CO oxidation (Han et al., 2006a, 2006b), oxidative removal of toluene (Deng et al., 2015), catalytic oxidation of benzene (An et al., 2013), and complete ethanol and toluene catalytic oxidation (Chen et al., 2020b). Kim and Shim (2010) compared the toluene oxidation activity of Mn<sub>2</sub>O<sub>3</sub> and MnO<sub>2</sub>, finding that the activity of Mn<sub>2</sub>O<sub>3</sub> ( $T_{50} = 280^\circ\text{C}$ ,  $T_{90} = 295^\circ\text{C}$ ) was higher than that of MnO<sub>2</sub> ( $T_{50} = 340^\circ\text{C}$ ,  $T_{90} = 375^\circ\text{C}$ ). Giving the outstanding catalytic oxidation performance of Mn<sub>2</sub>O<sub>3</sub>, therefore, we will optimize the Mn<sub>2</sub>O<sub>3</sub> material for the utilization of ethyl acetate oxidation in this work.

The use of different precursors would affect the catalytic performance, resulting from the change in the properties of catalysts, such as crystallinity, surface area, redox properties, and so on (Cai et al., 2012; Wang et al., 2015;

Wang and Li, 2010). For purpose of investigating the suitable precursor, the Mn<sub>2</sub>O<sub>3</sub> catalyst prepared with three different Mn precursors (MnCl<sub>2</sub>, Mn(CH<sub>3</sub>COO)<sub>2</sub> (abbreviated as MnAc<sub>2</sub>), MnSO<sub>4</sub>) was evaluated in the catalytic oxidation of ethyl acetate in this study. The catalytic activity was significantly different among the three Mn<sub>2</sub>O<sub>3</sub> catalysts. Compared to the Mn<sub>2</sub>O<sub>3</sub>-Ac and Mn<sub>2</sub>O<sub>3</sub>-SO<sub>4</sub>, the Mn<sub>2</sub>O<sub>3</sub>-Cl catalyst possessed the best catalytic performance, achieving almost 100% conversion of 1000 ppmV ethyl acetate only at 212°C. The morphology, structure, chemical state and redox properties of the three catalysts were systematically characterized by X-ray diffraction (XRD), N<sub>2</sub> adsorption-desorption isotherm, scanning electron microscopy (SEM), transmission electron microscopy (TEM), X-ray photoelectron spectroscopy (XPS), H<sub>2</sub> temperature-programmed reduction (H<sub>2</sub>-TPR), and O<sub>2</sub> temperature-programmed desorption (O<sub>2</sub>-TPD) measurements to elucidate behaviors of catalysts derived from various precursors.

## 1. Materials and methods

### 1.1. Catalyst synthesis

The manganese oxide materials were prepared by the homogeneous precipitation method. First, 0.3 mol/L MnCl<sub>2</sub>·4H<sub>2</sub>O, 0.3 mol/L MnAc<sub>2</sub>·4H<sub>2</sub>O, and 0.3 mol/L MnSO<sub>4</sub>·H<sub>2</sub>O, was dissolved in 370 mL deionized water under stirring, respectively. Subsequently, 2.7 mol/L urea was added into the above mixed solution. Finally, the mixed solution was maintained at 90°C for 24 hr followed by filtration, and the resulting precipitate was washed with deionized water. The solid product was dried at 100°C and then calcined at 500°C for 3 hr. The manganese oxides prepared with MnCl<sub>2</sub>·4H<sub>2</sub>O, MnAc<sub>2</sub>·4H<sub>2</sub>O, and MnSO<sub>4</sub>·H<sub>2</sub>O precursors were denoted as Mn<sub>2</sub>O<sub>3</sub>-Cl, Mn<sub>2</sub>O<sub>3</sub>-Ac, and Mn<sub>2</sub>O<sub>3</sub>-SO<sub>4</sub>, respectively.

### 1.2. Characterization

The XRD patterns of the catalysts were recorded by the XRD diffractometer (X'Pert Pro, PANalytical B.V., Netherlands) with Cu K $\alpha$  radiation ( $\lambda = 1.5406 \text{ \AA}$ ). N<sub>2</sub> physisorption analysis was measured at -196°C using an ASAP 2020 N instrument (Micromeritics, USA). The morphology of the catalysts was characterized by FE-SEM (S-4800, Hitachi, Japan). HR-TEM was performed on a JEOL JEM 2010 TEM (Hitachi, Japan) at 200 kV. The mass ratio S/Mn of the catalysts was analyzed using an inductively coupled plasma optical emission spectrometry (ICP-OES) (Varian700, Agilent, USA).

XPS measurements were performed on an ESCALAB250 (Thermo Fisher Scientific, USA) spectrometer equipped with a mono-chromated Al K $\alpha$  X-ray source (1486.6 eV). The H<sub>2</sub>-TPR measurements were used a Micromeritics AutoChem 2920 chemisorption analyzer (Micromeritics, USA) with a thermal conductivity detector (TCD) detector. About 60 mg catalysts were pretreated at 150°C for 1 hr in a flow of air (50 mL/min), and cooled the reactor to 30°C. The catalysts were heated to 700°C in a 5 vol.% H<sub>2</sub>/Ar at a ramp rate of 10°C/min. O<sub>2</sub>-TPD measurements were carried out with the same equipment

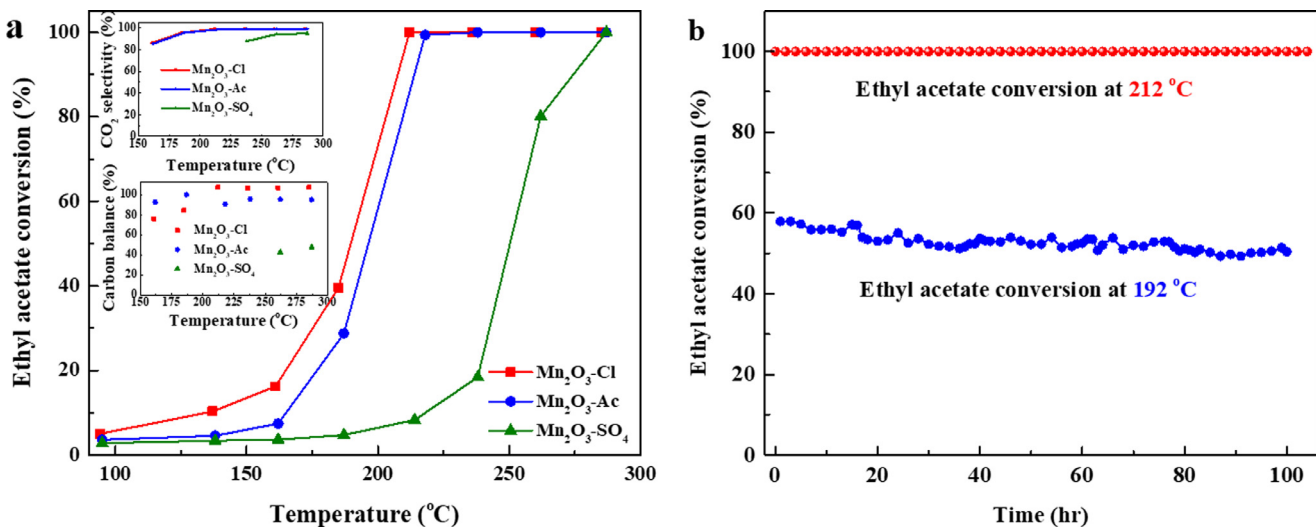


Fig. 1 – (a) Ethyl acetate conversion and (inset) CO<sub>2</sub> selectivity, (inset) carbon balance over different Mn<sub>2</sub>O<sub>3</sub> catalysts prepared with different precursors, (b) stability test for ethyl acetate oxidation with time-on-stream over Mn<sub>2</sub>O<sub>3</sub>-Cl catalysts. Reaction conditions: [Ethyl acetate] = 1000 ppmV, [O<sub>2</sub>] = 20 vol.%, gas hourly space velocity (GHSV) = 78,000 hr<sup>-1</sup>. Mn<sub>2</sub>O<sub>3</sub>-Cl: Mn<sub>2</sub>O<sub>3</sub> prepared with MnCl<sub>2</sub>; Mn<sub>2</sub>O<sub>3</sub>-Ac: Mn<sub>2</sub>O<sub>3</sub> prepared with Mn(CH<sub>3</sub>COO)<sub>2</sub>; Mn<sub>2</sub>O<sub>3</sub>-SO<sub>4</sub>: Mn<sub>2</sub>O<sub>3</sub> prepared with MnSO<sub>4</sub>.

with the H<sub>2</sub>-TPR. A 100 mg sample was pre-treated in He at 300°C for 1 hr, then cooled down to room temperature, and saturated with 5 vol.% O<sub>2</sub>/He mixture gas for 1 hr. Finally, the temperature was raised in He flow at a rate of 10°C/min to 1000°C. The products were monitored by a mass spectroscopy (MS) (LC-D200M PRO, Tilon, USA).

### 1.3. Catalytic tests of VOC oxidation

The catalytic oxidation experiments for ethyl acetate were conducted in a fixed-bed quartz reactor in the range of 150–400°C. Reaction conditions were as follows: 200 mg catalyst; 1000 ppmV ethyl acetate, 20 vol.% O<sub>2</sub>, N<sub>2</sub> balance, 300 mL/min; gas hourly space velocity (GHSV) = 78,000 hr<sup>-1</sup>. The ethyl acetate, CO<sub>2</sub>, and CO concentration were analyzed online by a gas chromatograph (Agilent 7890B, Agilent, USA, HP-5 capillary column). The detection accuracy was about 1 ppmV. The ethyl acetate conversion was calculated following Eq. (1):

$$\text{Conversion (\%)} = \left( 1 - \frac{[\text{Ethyl acetate}]_{\text{out}}}{[\text{Ethyl acetate}]_{\text{in}}} \right) \times 100\% \quad (1)$$

The CO<sub>2</sub> selectivity was defined as Eq. (2):

$$\text{CO}_2 \text{ selectivity (\%)} = \frac{[\text{CO}_2]_{\text{out}}}{[\text{CO}_2]_{\text{out}} + [\text{CO}]_{\text{out}}} \times 100\% \quad (2)$$

The main products from the test were CO and CO<sub>2</sub>, so the carbon balance was calculated by Eq. (3):

$$\text{Carbon balance (\%)} = \frac{[\text{CO}]_{\text{out}} + [\text{CO}_2]_{\text{out}}}{4 \times ([\text{Ethyl acetate}]_{\text{in}} - [\text{Ethyl acetate}]_{\text{out}})} \times 100\% \quad (3)$$

## 2. Results

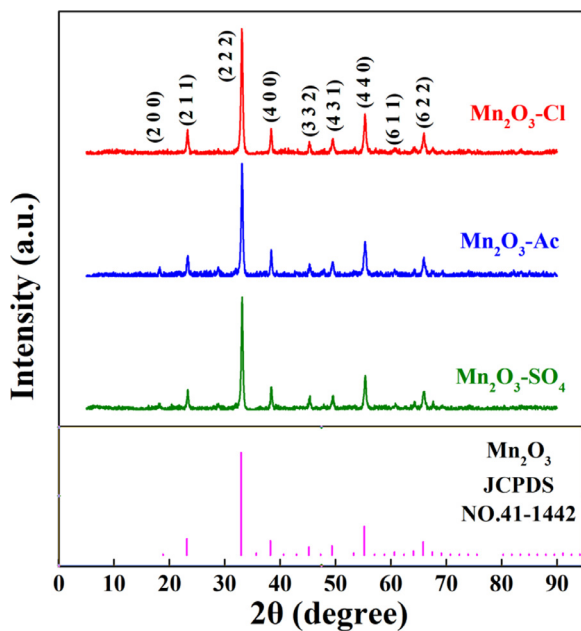
### 2.1. Catalytic performance

Fig. 1a compares the ethyl acetate conversion over Mn<sub>2</sub>O<sub>3</sub> catalysts prepared with different precursors as a function of reaction temperature. It was apparent that the catalytic performance of Mn<sub>2</sub>O<sub>3</sub>-SO<sub>4</sub> was the worst, approaching 90% ethyl acetate conversion at 274°C. The activity of Mn<sub>2</sub>O<sub>3</sub>-Ac was much better, with the T<sub>50</sub> and T<sub>90</sub> at 197 and 215°C, respectively. Mn<sub>2</sub>O<sub>3</sub>-Cl possessed the highest catalytic activity, with T<sub>90</sub> of 206°C, which was 69°C lower than that of Mn<sub>2</sub>O<sub>3</sub>-SO<sub>4</sub>. In addition, the CO<sub>2</sub> selectivity in the inset of Fig. 1a revealed that the Mn<sub>2</sub>O<sub>3</sub>-Cl and Mn<sub>2</sub>O<sub>3</sub>-Ac catalysts possessed higher CO<sub>2</sub> selectivity than Mn<sub>2</sub>O<sub>3</sub>-SO<sub>4</sub>. Meanwhile, the Mn<sub>2</sub>O<sub>3</sub>-Cl owned the most stable carbon balance.

The stability of Mn<sub>2</sub>O<sub>3</sub>-Cl catalyst (the optimal catalysts mentioned above) was tested, and the evolution of ethyl acetate conversion with time-on-stream is shown in Fig. 1b. During the period of 106 hr test at 212°C, the removal rate of ethyl acetate over the Mn<sub>2</sub>O<sub>3</sub>-Cl catalyst was well sustained at 100% without noticeable activity loss. Meanwhile, in order to comprehensively investigate the stability of the Mn<sub>2</sub>O<sub>3</sub>-Cl catalyst, the conversion of ethyl acetate at 192°C was measured continuously for about 100 hr, and the catalytic activity slightly dropped. The above results indicated the Mn<sub>2</sub>O<sub>3</sub>-Cl catalyst possessed outstanding durability.

### 2.2. Crystalline and morphological structure of catalysts

XRD was carried out to investigate the crystalline phases of the prepared catalysts, and the XRD patterns are shown in Fig. 2. The peaks at  $2\theta = 18.9^\circ, 23.1^\circ, 33.0^\circ, 38.2^\circ, 45.2^\circ, 49.4^\circ, 55.2^\circ, 60.6^\circ$ , and  $65.8^\circ$  were assigned to the (200), (211), (222),



**Fig. 2 – Powder XRD of  $\text{Mn}_2\text{O}_3$  catalysts prepared with different precursors.**

**Table 1 – Surface area, pore volume and crystallite size of  $\text{Mn}_2\text{O}_3$  prepared with precursors.**

Sample	Surface area ( $\text{m}^2/\text{g}$ )	Pore diameter (nm)	Crystallite size (nm)
$\text{Mn}_2\text{O}_3\text{-Cl}$	41.1	11.39	23.6
$\text{Mn}_2\text{O}_3\text{-Ac}$	43.7	19.29	24.5
$\text{Mn}_2\text{O}_3\text{-SO}_4$	29.7	25.08	24.9

Crystallite size: calculated by the Scherrer equation at  $2\theta = 33^\circ$ .

(400), (332), (431), (440), (611), and (622) lattice planes of  $\text{Mn}_2\text{O}_3$ , respectively (JCPDS 41-1442) (Zhang et al., 2017; Zhao et al., 2018). Using the Scherrer equation for the peak due to the (222) plane, the crystallite size of all the  $\text{Mn}_2\text{O}_3$  catalysts was calculated (Table 1), giving values to be 23.6, 24.5, 24.9 nm for  $\text{Mn}_2\text{O}_3\text{-Cl}$ ,  $\text{Mn}_2\text{O}_3\text{-Ac}$ , and  $\text{Mn}_2\text{O}_3\text{-SO}_4$ , respectively. The XRD analysis confirmed that the facile homogeneous precipitation employed in this study was favorable for the formation of  $\text{Mn}_2\text{O}_3$ , and the precursors had little effects on the crystal phase and size.

The morphologies and structures of  $\text{Mn}_2\text{O}_3$  were obtained by SEM and HR-TEM (Fig. 3). As shown in Fig. 3a, all of the samples consisted of large quantities of cubes, similar to the results of a previous study by Lei et al. (2006), regardless of the precursor used. The HR-TEM analyses for all catalysts are presented in Fig. 3b. The apparent lattice spacing of 0.27 nm were ascribed to the (222) plane of  $\text{Mn}_2\text{O}_3$  (Biswas et al., 2015), in consistence with the XRD results.

The isotherms of the three catalysts displayed a type IV isotherm with H1-type hysteresis loop (shown in Fig. 4), indicating that all the samples are typical mesoporous materials (Shu et al., 2018). Compared with  $\text{Mn}_2\text{O}_3\text{-Cl}$ , the hysteresis

loops of  $\text{Mn}_2\text{O}_3\text{-Ac}$  and  $\text{Mn}_2\text{O}_3\text{-SO}_4$  were closer to relative pressure ( $P/P_0 = 1$ ), suggesting that some small pores were blocked and large pores were formed in their pore structures (Fang et al., 2015). The pore size distribution (the inset in Fig. 4) testifies that the pore diameters of  $\text{Mn}_2\text{O}_3\text{-Cl}$ ,  $\text{Mn}_2\text{O}_3\text{-Ac}$ , and  $\text{Mn}_2\text{O}_3\text{-SO}_4$  were 11.39, 19.29 and 25.08 nm, respectively. Table 1 lists the surface area, pore diameter and crystallite size of the catalysts. The Brunner–Emmet–Teller (BET) surface areas followed the order:  $\text{Mn}_2\text{O}_3\text{-Ac}$  ( $43.7 \text{ m}^2/\text{g}$ ) >  $\text{Mn}_2\text{O}_3\text{-Cl}$  ( $41.1 \text{ m}^2/\text{g}$ ) >  $\text{Mn}_2\text{O}_3\text{-SO}_4$  ( $29.7 \text{ m}^2/\text{g}$ ).

### 2.3. Chemical states and oxygen species of catalysts

The XPS measurements were used to investigate the composition and oxidation state. As shown in Fig. 5a, over all the samples two obvious peaks were observed at 641.6 and 653.3 eV, which assigned to  $\text{Mn} 2p_{3/2}$  and  $\text{Mn} 2p_{1/2}$ , separately. The results are consistent with previously reported data, confirming that all the catalysts were  $\text{Mn}_2\text{O}_3$  (Stranick, 1999). The average oxidation state (AOS) of the surface Mn in the manganese oxide could be calculated by the formula:  $\text{AOS} = 8.956 - 1.126\Delta E$  ( $\Delta E$  is the splitting width of  $\text{Mn} 3s$ ) (Santos et al., 2009). The AOS values of all the  $\text{Mn}_2\text{O}_3$  catalysts were 3.12, 3.04, and 2.83, with  $\text{Mn}_2\text{O}_3\text{-Cl} > \text{Mn}_2\text{O}_3\text{-Ac} > \text{Mn}_2\text{O}_3\text{-SO}_4$ , respectively (Fig. 5b). Obviously, the AOS values of the catalysts are closely correlated with the corresponding catalytic activities, same as the previous study reported by Santos et al. (2009).

The XPS results of O 1s in  $\text{Mn}_2\text{O}_3$  catalysts are shown in Fig. 6. The peak at 529.7 eV was ascribed to the lattice oxygen (marked as  $O_{\text{latt}}$ ), while the signal at 531.3 eV was assigned to the surface adsorbed oxygen (marked as  $O_{\text{surf}}$ ) (Zhang et al., 2015). The ratios  $O_{\text{latt}}/O_{\text{surf}}$  were calculated and summarized in Fig. 6. The  $O_{\text{latt}}/O_{\text{surf}}$  ratios followed the sequence  $\text{Mn}_2\text{O}_3\text{-Cl}$  (3.23) >  $\text{Mn}_2\text{O}_3\text{-Ac}$  (2.91) >  $\text{Mn}_2\text{O}_3\text{-SO}_4$  (2.12). The oxygen temperature-programmed desorption ( $\text{O}_2\text{-TPD}$ ) experiment has been carried out to investigate the oxygen species (shown in Fig. 6b). All catalysts exhibited a broad peak below  $650^\circ\text{C}$  and a prominent desorption peak at around  $850^\circ\text{C}$ , which were attributed to surface oxygen and lattice oxygen, separately (Liu et al., 2017). According to the results of  $\text{O}_2\text{-TPD}$ , the amount of lattice oxygen species on three  $\text{Mn}_2\text{O}_3$  catalysts was calculated by integral area of the peak at around  $850^\circ\text{C}$ , and the results were shown in Fig. 6b. Obviously, the amount of lattice oxygen species followed the same sequence with the  $O_{\text{latt}}/O_{\text{surf}}$  ratios (in Fig. 6a):  $\text{Mn}_2\text{O}_3\text{-Cl}$  (142) >  $\text{Mn}_2\text{O}_3\text{-Ac}$  (121) >  $\text{Mn}_2\text{O}_3\text{-SO}_4$  (89).

Minicò et al. (2000) have observed that the high activity of  $\text{Au}/\text{Fe}_2\text{O}_3$  towards VOC oxidation could be attributed to the high dispersion of Au which weakened the Fe-O bond and thus increased the mobility of lattice oxygen, which was probably involved in the VOC oxidation through a Mars-van Krevelen mechanism. Zhang et al. (2015) found that the performance of  $\text{MnO}_2$  catalyst with different crystal structures in HCHO oxidation was also closely interrelated to the amounts of  $O_{\text{latt}}$  species. In this study, the lattice oxygen concentration of the  $\text{Mn}_2\text{O}_3$  catalysts was related to the activity of the catalysts, indicating that the lattice oxygen was of great importance in oxidizing the ethyl acetate.

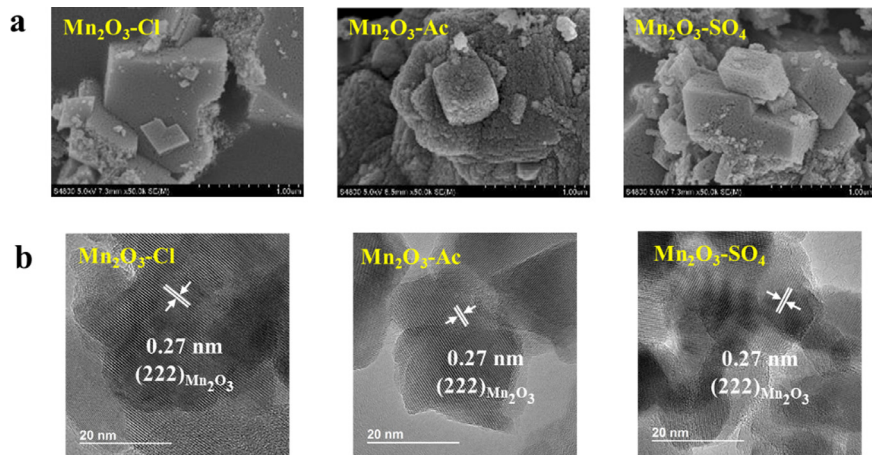


**Fig. 3 – (a) Scanning electron microscopy (SEM) and (b) high resolution transmission electron microscopy (HR-TEM) images of Mn<sub>2</sub>O<sub>3</sub> catalysts prepared with different precursors.**

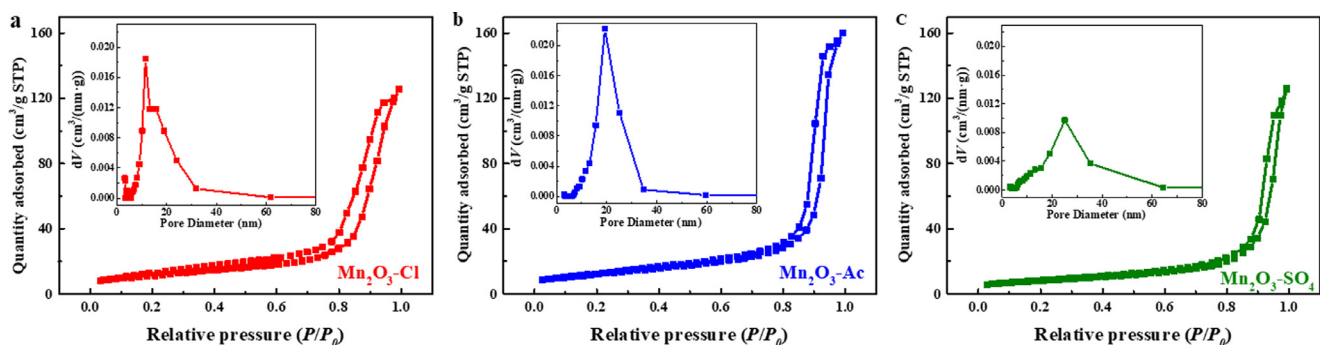


**Fig. 4 – N<sub>2</sub> adsorption-desorption isotherms and the pore size distribution plots (inset) of Mn<sub>2</sub>O<sub>3</sub> catalysts prepared with (a) Mn<sub>2</sub>O<sub>3</sub>-Cl, (b) Mn<sub>2</sub>O<sub>3</sub>-Ac, and (c) Mn<sub>2</sub>O<sub>3</sub>-SO<sub>4</sub>. dV: pore volume per unit diameter; STP: standard temperature and pressure.**

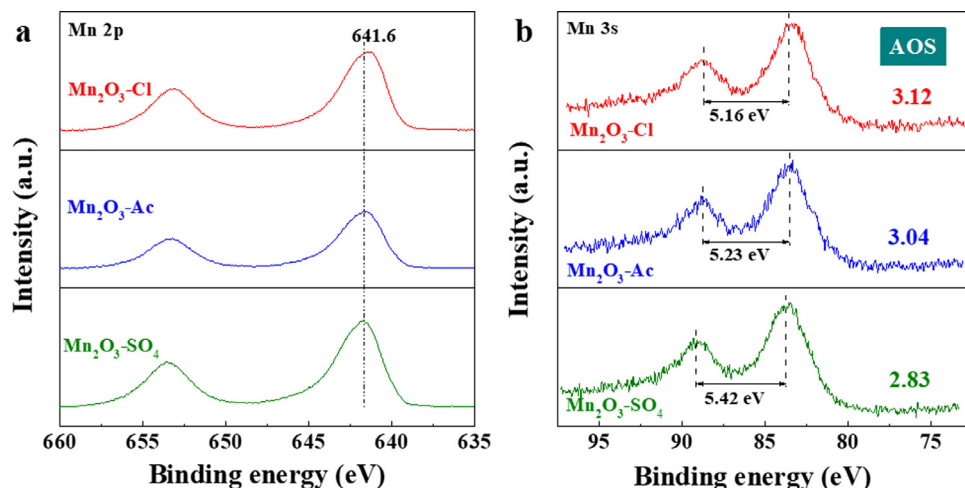


**Fig. 5 – X-ray photoelectron spectroscopy (XPS) results of (a) Mn 2p and (b) Mn 3s in Mn<sub>2</sub>O<sub>3</sub> catalysts. AOS: average oxidation state.**

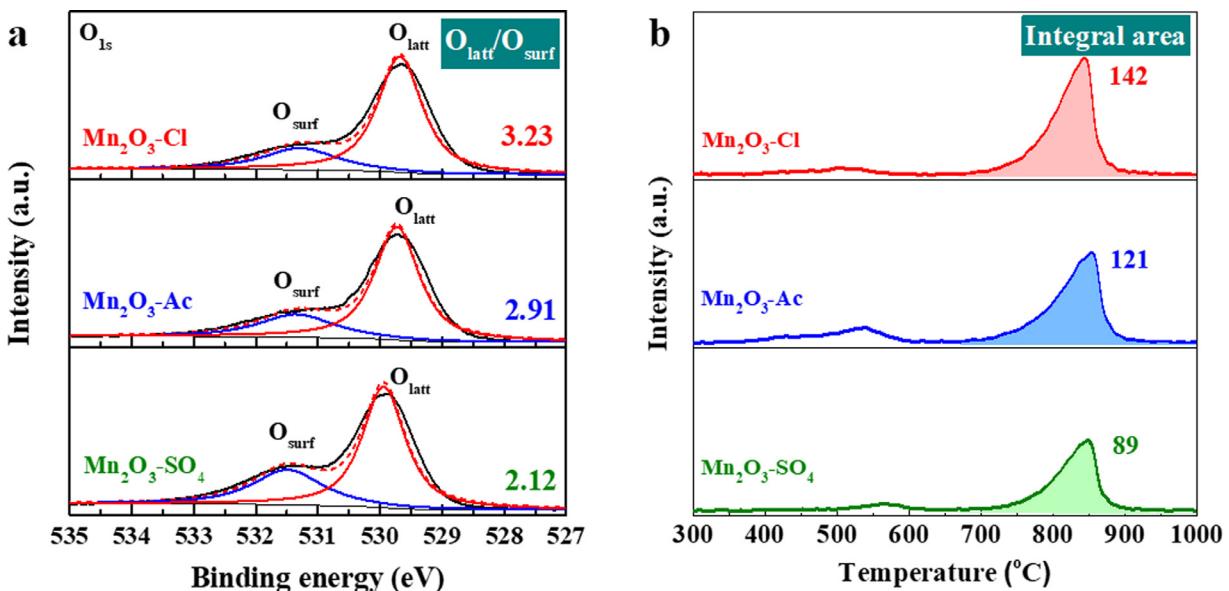


Fig. 6 – XPS results of (a) O 1s and (b) O<sub>2</sub> temperature-programmed desorption (O<sub>2</sub>-TPD) results in Mn<sub>2</sub>O<sub>3</sub> catalysts. O<sub>latt</sub>: lattice oxygen; O<sub>surf</sub>: surface adsorbed oxygen.

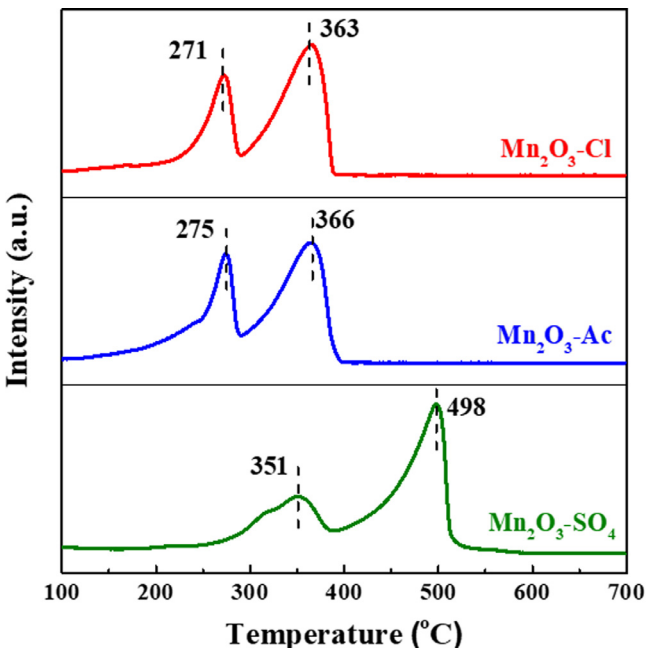


Fig. 7 – H<sub>2</sub> temperature-programmed reduction (H<sub>2</sub>-TPR) results of Mn<sub>2</sub>O<sub>3</sub> catalysts prepared with different precursors.

#### 2.4. Reducibility of catalysts

H<sub>2</sub>-TPR was measured to investigate the reducibility of the three Mn<sub>2</sub>O<sub>3</sub> catalysts, and the results are presented in Fig. 7. All of the Mn<sub>2</sub>O<sub>3</sub> catalysts displayed two peaks: the first reduction peak at low temperature was ascribed to the second reductive transition of Mn<sub>2</sub>O<sub>3</sub> to Mn<sub>3</sub>O<sub>4</sub>, while the peak at high temperature was attributed to the reductive transi-

tion of Mn<sub>3</sub>O<sub>4</sub> to MnO (Biswas et al., 2015; Tang et al., 2006; Zhang et al., 2017). The temperature of the first reduction peak on Mn<sub>2</sub>O<sub>3</sub>-Cl catalyst was the lowest (271°C), followed by Mn<sub>2</sub>O<sub>3</sub>-Ac (275°C), and Mn<sub>2</sub>O<sub>3</sub>-SO<sub>4</sub> (351°C). Similarly, the temperatures of the second reduction peak on Mn<sub>2</sub>O<sub>3</sub> catalysts were in the same order. Judging from the temperature order of the reduction peak, the reducibility of all the Mn<sub>2</sub>O<sub>3</sub> samples followed the trend: Mn<sub>2</sub>O<sub>3</sub>-Cl > Mn<sub>2</sub>O<sub>3</sub>-Ac > Mn<sub>2</sub>O<sub>3</sub>-SO<sub>4</sub>, indicating that Mn<sub>2</sub>O<sub>3</sub>-Cl had stronger redox properties. The reducibility measured by H<sub>2</sub>-TPR could reflect the oxygen mobility in the samples (Zhao et al., 2020): since the temperature of the first reduction peak on Mn<sub>2</sub>O<sub>3</sub>-Cl catalyst was the lowest, proving that the Mn<sub>2</sub>O<sub>3</sub>-Cl possessed the most mobile oxygen species among the three catalysts. Consequently, high oxygen mobility of Mn<sub>2</sub>O<sub>3</sub>-Cl catalyst leads to more oxygen being adsorbed and then exciting to active oxygen species, which would promote the catalytic oxidation reaction.

## 3. Discussion

### 3.1. Effect of physical properties of catalysts on catalytic performance

The ethyl acetate conversion over all the Mn<sub>2</sub>O<sub>3</sub> catalysts was strongly dependent on the precursor. According to the results of XRD, SEM, and TEM, it was obvious to find that the use of different precursors had no obvious effect on the structure and morphology of Mn<sub>2</sub>O<sub>3</sub> catalysts. That is to say, there is little correlation between the structure and morphology of Mn<sub>2</sub>O<sub>3</sub> catalysts and catalytic activity. Besides, Mn<sub>2</sub>O<sub>3</sub>-Ac owed the largest BET surface area (Table 1), while Mn<sub>2</sub>O<sub>3</sub>-Cl possessed the best activity for ethyl acetate oxidation (Fig. 1a), manifesting that the surface area was not also the determining factor

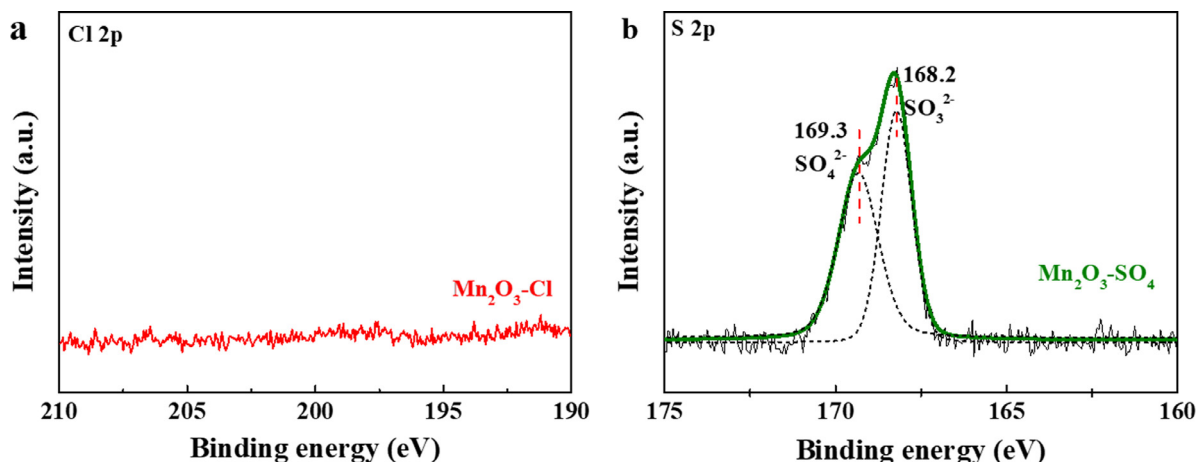


Fig. 8 – XPS results of (a) Cl 2p in Mn<sub>2</sub>O<sub>3</sub>-Cl catalysts and (b) S 2p in Mn<sub>2</sub>O<sub>3</sub>-SO<sub>4</sub> catalysts.

in the ethyl acetate oxidation. From the above analysis, we can know that the effect of physical properties of Mn<sub>2</sub>O<sub>3</sub> catalysts was marginal.

### 3.2. Effect of surface deposition species of catalysts on catalytic performance

Previous studies showed that the chlorine deposited on the catalyst surface is a primary cause for catalyst deactivation (Lopez et al., 2006; Kamal et al., 2016). So, the presence of chlorine in Mn<sub>2</sub>O<sub>3</sub> catalysts was measured by XPS, and the results are shown in Fig. 8a. The characteristic chlorine peak did not appear in the spectra of Mn<sub>2</sub>O<sub>3</sub>-Cl, indicating that chlorine does not exist on the surface of the Mn<sub>2</sub>O<sub>3</sub> catalyst produced with the MnCl<sub>2</sub> precursor.

Meanwhile, XPS measurements were also carried out to investigate the sulfur content (Fig. 8b). Clearly, the characteristic peaks of S were only observed for the Mn<sub>2</sub>O<sub>3</sub>-SO<sub>4</sub> catalyst. The peak at 169.3 eV was attributed to SO<sub>4</sub><sup>2-</sup>, while the peak at 168.2 eV was due to SO<sub>3</sub><sup>2-</sup> (Wu et al., 2009). In order to determine whether surface sulfates deactivate the Mn<sub>2</sub>O<sub>3</sub>-SO<sub>4</sub> catalyst, the surface sulfates were removed through treatment with NH<sub>3</sub> at 480°C as reported by Lian et al. (2020). The ICP results in the inset of Fig. 9a verified that after NH<sub>3</sub> treatment the surface sulfate content of the Mn<sub>2</sub>O<sub>3</sub>-SO<sub>4</sub> catalyst decreased dramatically. However, contrary to our expectations, the ethyl acetate conversion of the Mn<sub>2</sub>O<sub>3</sub>-SO<sub>4</sub> catalyst treated by NH<sub>3</sub> did not improve, but instead slightly decreased (shown in Fig. 9). Therefore, the presence of sulfur on the Mn<sub>2</sub>O<sub>3</sub>-SO<sub>4</sub> catalyst has little influence on the catalytic performance. As mentioned in Section 2.3, the activity of the catalysts was correlated with the average oxidation state of the manganese oxides. In order to study the effects of NH<sub>3</sub> treatment on the average oxidation state of Mn<sub>2</sub>O<sub>3</sub>-SO<sub>4</sub> catalyst, the XPS was measured and the result of Mn 3s in Mn<sub>2</sub>O<sub>3</sub>-SO<sub>4</sub> catalyst was shown in Fig. 9b. It was clear to observe that the AOS value of Mn<sub>2</sub>O<sub>3</sub>-SO<sub>4</sub> catalyst treated by NH<sub>3</sub> was similar with that of the Mn<sub>2</sub>O<sub>3</sub>-SO<sub>4</sub> catalyst indicating that the NH<sub>3</sub> treatment had no influence on the catalyst. Through the above analysis, the influence of residual Cl or S on the catalytic performance could be completely excluded.

### 3.3. Effect of chemical properties of catalysts on catalytic performance

As described in the previous literatures, the Mars-van Krevelen mechanism, occurred in some oxidation reactions on MnO<sub>x</sub> catalysts, implied that the lattice oxygen could play an important role during the reaction (Song and Hensen, 2013; Xu et al., 2006; Zhang et al., 2015). Tang et al. (2006) have found that the lattice oxygen in MnO<sub>x</sub>-CeO<sub>2</sub> catalysts was beneficial for HCHO oxidation. Chen et al. (2020a) quantitatively correlated the concentration of oxygen species with the reaction rates in benzene oxidation, and suggested that surface lattice oxygen species were decisive during the oxidation reaction. The key role of surface lattice oxygen was further proved by the Isotopic experiments: the surface lattice oxygen firstly oxidized the C<sub>6</sub>H<sub>6</sub>, and simultaneously produced the oxygen vacancies which could be subsequently refilled by gas-phase O<sub>2</sub>.

In this work, it is interesting to note that a good linear correlation exists between the ratio of O<sub>latt</sub>/O<sub>surf</sub> and the ethyl acetate conversion, as shown in Fig. 10a. The linear relationship provides clear evidence that lattice oxygen species played the key role in the ethyl acetate oxidation. The importance of the lattice oxygen species was further confirmed by the good linearity between the integral area of the lattice oxygen and the catalytic activity toward ethyl acetate (Fig. 10b). Furthermore, a close linear correlation between the low initial reduction temperature and ethyl acetate conversion was also drawn, as shown in Fig. 10b. The low initial reduction temperature indicates that the catalyst has stronger oxygen mobility, so more oxygen species could participate in the oxidation reaction, thus possessing much better catalytic performance.

On the basis of the above discussions, we summarize the schematic illustration of ethyl acetate oxidation following Mars-van-Krevelen mechanism over Mn<sub>2</sub>O<sub>3</sub> catalysts (Fig. 11). Firstly, the ethyl acetate adsorbs at the lattice oxygen and is oxidized, while the Mn cations are reduced and oxygen participated in the reaction to produce the CO<sub>2</sub> and H<sub>2</sub>O, and then forming the oxygen vacancies (green circles in the Fig. 11); finally, the reduced catalyst is re-oxidized, while the lattice oxygen of catalyst is replenished by gaseous oxygen. Moreover, the strong oxygen mobility could promote more oxy-

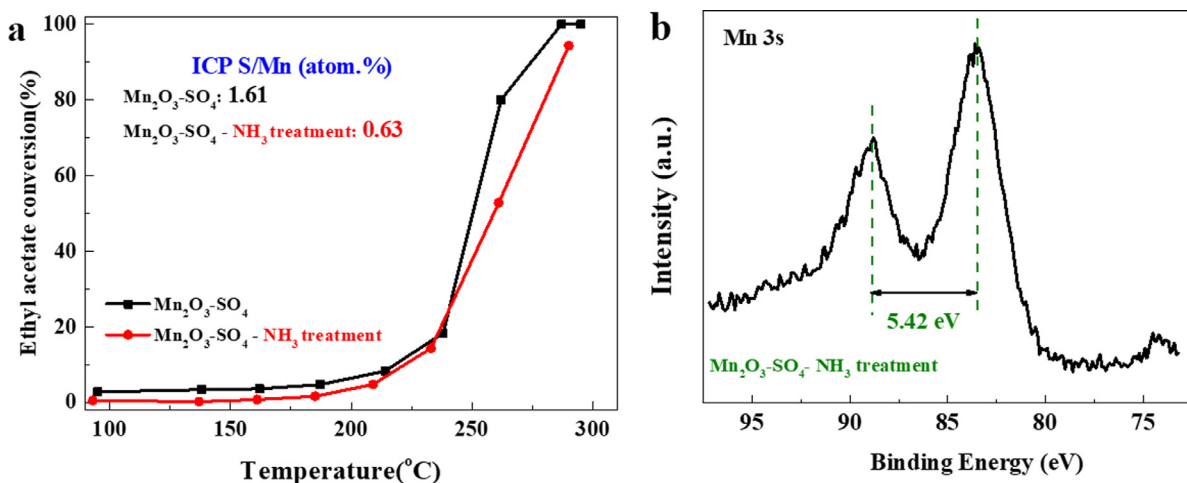


Fig. 9 – (a) Ethyl acetate conversion over Mn<sub>2</sub>O<sub>3</sub>-SO<sub>4</sub> and Mn<sub>2</sub>O<sub>3</sub>-SO<sub>4</sub> treated by NH<sub>3</sub> and (b) XPS result of Mn 3s in Mn<sub>2</sub>O<sub>3</sub>-SO<sub>4</sub> catalyst treated with NH<sub>3</sub>. ICP: inductively coupled plasma.

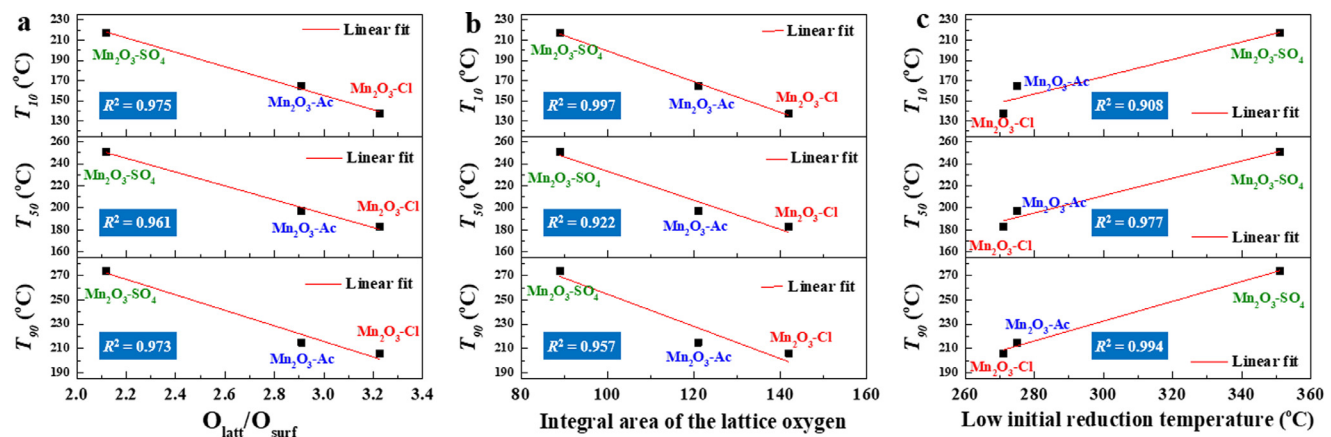


Fig. 10 – Relationship between (a) the ratio of O<sub>latt</sub>/O<sub>surf</sub> and the catalytic activity toward ethyl acetate; (b) the integral area of the lattice oxygen and the catalytic activity toward ethyl acetate, and (c) the low initial reduction temperature and the catalytic activity toward ethyl acetate. T<sub>x</sub>: the temperature at which a conversion of x% was obtained.

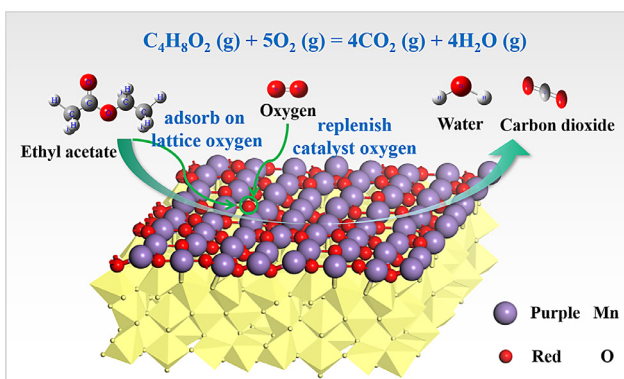


Fig. 11 – Scheme of the ethyl acetate oxidation reaction over Mn<sub>2</sub>O<sub>3</sub> catalysts.

gen species taking part in ethyl acetate oxidation. Therefore, the Mn<sub>2</sub>O<sub>3</sub>-Cl, owing more lattice oxygen species and stronger

oxygen mobility, exhibited higher catalytic activity than the other two catalysts.

#### 4. Conclusions

The effects of different precursors on the structure and ethyl acetate catalytic oxidation activity of Mn<sub>2</sub>O<sub>3</sub> catalysts were investigated in this study. The Mn<sub>2</sub>O<sub>3</sub> catalysts prepared using MnCl<sub>2</sub> as precursor displayed higher ethyl acetate conversion and CO<sub>2</sub> selectivity than catalysts prepared using MnSO<sub>4</sub> or MnAc<sub>2</sub>. Moreover, the Mn<sub>2</sub>O<sub>3</sub>-Cl catalyst still maintained close to 100% conversion at 212°C after 106 hr. For all the Mn<sub>2</sub>O<sub>3</sub> catalysts, the amount of lattice oxygen species was linearly correlated with the ethyl acetate catalytic oxidation activity. The relationship showed that lattice oxygen species on the catalyst surface are essential to the high catalytic performance. The results of H<sub>2</sub>-TPR revealed that the reducibility of the Mn<sub>2</sub>O<sub>3</sub> samples followed the trend: Mn<sub>2</sub>O<sub>3</sub>-Cl > Mn<sub>2</sub>O<sub>3</sub>-Ac > Mn<sub>2</sub>O<sub>3</sub>-SO<sub>4</sub>. In other words, Mn<sub>2</sub>O<sub>3</sub>-Cl possessed the highest oxygen

mobility, promoting more active oxygen involved in the ethyl acetate oxidation reaction. This study can improve our understanding of ethyl acetate oxidation on  $Mn_2O_3$  catalysts and serve as a guide in using  $Mn_2O_3$  for removal of ethyl acetate.

## Declaration of competing interest

The authors declare that they have no competing, personal and financial interests in this manuscript.

## Acknowledgments

The work was supported by the National Key R&D Program of China (No. 2017YFE0127500).

## REFERENCES

- An, H.B., Kim, J.M., Jurng, J., Bae, G.N., Jeon, J.K., Park, S.H., et al., 2013. Catalytic oxidation of benzene using mesoporous alpha- $Mn_2O_3$ . *J. Nanosci. Nanotechnol.* 13, 7472–7476.
- Bastos, S.S.T., Órfão, J.J.M., Freitas, M.M.A., Pereira, M.F.R., Figueiredo, J.L., 2009. Manganese oxide catalysts synthesized by exotemplating for the total oxidation of ethanol. *Appl. Catal. B Environ.* 93, 30–37.
- Biswas, S., Poyraz, A.S., Meng, Y., Kuo, C.H., Guild, C., Tripp, H., et al., 2015. Ion induced promotion of activity enhancement of mesoporous manganese oxides for aerobic oxidation reactions. *Appl. Catal. B Environ.* 165, 731–741.
- Cai, L.N., Guo, Y., Lu, A.H., Branton, P., Li, W.C., 2012. The choice of precipitant and precursor in the co-precipitation synthesis of copper manganese oxide for maximizing carbon monoxide oxidation. *J. Mol. Catal. A Chem.* 360, 35–41.
- Chen, B.B., Wu, B., Yu, L.M., Crocker, M., Shi, C., 2020a. Investigation into the catalytic roles of various oxygen species over different crystal phases of  $MnO_2$  for  $C_6H_6$  and  $HCHO$  oxidation. *ACS Catal.* 10, 6176–6187.
- Chen, S.H., Li, H., Hao, Y., Chen, R., Chen, T.H., 2020b. Porous Mn-based oxides for complete ethanol and toluene catalytic oxidation: the relationship between structure and performance. *Catal. Sci. Technol.* 10, 1941–1951.
- Deng, J., He, S., Xie, S., Yang, H., Liu, Y., Guo, G., et al., 2015. Ultralow loading of silver nanoparticles on  $Mn_2O_3$  nanowires derived with molten salts: a high-efficiency catalyst for the oxidative removal of toluene. *Environ. Sci. Technol.* 49, 11089–11095.
- Deng, J., Zhang, L., Dai, H., Au, C.T., 2009. In situ hydrothermally synthesized mesoporous  $LaCoO_3/SBA-15$  catalysts: high activity for the complete oxidation of toluene and ethyl acetate. *Appl. Catal. A Gen.* 352, 43–49.
- Djinovic, P., Ristic, A., Zumboar, T., Dasireddy, V., Rangus, M., Drazic, G., et al., 2020. Synergistic effect of  $CuO$  nanocrystals and Cu-oxo-Fe clusters on silica support in promotion of total catalytic oxidation of toluene as a model volatile organic air pollutant. *Appl. Catal. B Environ.* 268, 118749.
- Everaert, K., Baeyens, J., 2004. Catalytic combustion of volatile organic compounds. *J. Hazard. Mater.* 109, 113–139.
- Fang, Z., Yuan, B., Lin, T., Xu, H., Cao, Y., Shi, Z., et al., 2015. Monolith  $Ce_{0.65}Zr_{0.35}O_2$ -based catalysts for selective catalytic reduction of NO with  $NH_3$ . *Chem. Eng. Res. Des.* 94, 648–659.
- Fu, Z., Liu, L., Song, Y., Ye, Q., Cheng, S., Kang, T., et al., 2017. Catalytic oxidation of carbon monoxide, toluene, and ethyl acetate over the  $xPd/OMS-2$  catalysts: effect of Pd loading. *Front. Chem. Eng.* 11, 185–196.
- Guo, H., Zhang, Z.X., Hojo, H., Chen, M.X., Einaga, H., Shangguan, W., 2019. Catalytic removal of benzene at mild temperature over manganese oxide catalysts. *Catal. Surv. Asia* 23, 199–209.
- Han, Y.F., Chen, F., Zhong, Z.Y., Ramesh, K., Widjaja, E., Chen, L.W., 2006a. Synthesis and characterization of  $Mn_3O_4$  and  $Mn_2O_3$  nanocrystals on SBA-15: novel combustion catalysts at low reaction temperatures. *Catal. Commun.* 7, 739–744.
- Han, Y.F., Chen, F., Zhong, Z., Ramesh, K., Chen, L., Widjaja, E., 2006b. Controlled synthesis, characterization, and catalytic properties of  $Mn_2O_3$  and  $Mn_3O_4$  nanoparticles supported on mesoporous silica SBA-15. *J. Phys. Chem. B* 110, 24450–24456.
- He, H., Wang, Z., Xu, M., He, Z., Song, S., 2012. Studies on the emission characteristics and countermeasures of VOCs from pharmaceutical industry-based on Zhejiang Province. *China Environ. Sci.* 32, 2271–2277.
- Huang, N., Qu, Z.P., Dong, C., Qin, Y., Duan, X.X., 2018. Superior performance of  $\alpha@beta-MnO_2$  for the toluene oxidation: active interface and oxygen vacancy. *Appl. Catal. A Gen.* 560, 195–205.
- Huang, S.Y., Zhang, C.B., He, H., 2013. Effect of pretreatment on  $Pd/Al_2O_3$  catalyst for catalytic oxidation of o-xylene at low temperature. *J. Environ. Sci.* 25, 1206–1212.
- Jia, J., Lu, X.L., Chen, C., He, M., Huang, H., 2020. Potassium-modulated  $\delta-MnO_2$  as robust catalysts for formaldehyde oxidation at room temperature. *Appl. Catal. B Environ.* 260, 118210–118221.
- Jiang, Y., Gao, J., Zhang, Q., Liu, Z., Fu, M., Wu, J., et al., 2019. Enhanced oxygen vacancies to improve ethyl acetate oxidation over  $MnO_x-CeO_2$  catalyst derived from MOF template. *Chem. Eng. J.* 371, 78–87.
- Kim, S.C., Shim, W.G., 2010. Catalytic combustion of VOCs over a series of manganese oxide catalysts. *Appl. Catal. B Environ.* 98, 180–185.
- Lei, S., Tang, K., Fang, Z., Liu, Q., Zheng, H., 2006. Preparation of  $\alpha-Mn_2O_3$  and  $MnO$  from thermal decomposition of  $MnCO_3$  and control of morphology. *Mater. Lett.* 60, 53–56.
- Li, S., Hao, Q., Zhao, R., Liu, D., Duan, H., Dou, B., 2016. Highly efficient catalytic removal of ethyl acetate over Ce/Zr promoted copper/ZSM-5 catalysts. *Chem. Eng. J.* 285, 536–543.
- Lian, Z., Xin, S., Zhu, N., Wang, Q., Xu, J., Zhang, Y., et al., 2020. Effect of treatment atmosphere on the vanadium species of  $V/TiO_2$  catalysts for the selective catalytic reduction of  $NO_x$  with  $NH_3$ . *Catal. Sci. Technol.* 10, 311–314.
- Liu, L., Song, Y., Fu, Z., Ye, Q., Cheng, S., Kang, T., et al., 2017. Effect of preparation method on the surface characteristics and activity of the  $Pd/OMS-2$  catalysts for the oxidation of carbon monoxide, toluene, and ethyl acetate. *Appl. Surf. Sci.* 396, 599–608.
- Lopez, E., Ordóñez, S., Diez, F., 2006. Deactivation of a  $Pd/Al_2O_3$  catalyst used in hydrodechlorination reactions: influence of the nature of organochlorinated compound and hydrogen chloride. *Appl. Catal. B Environ.* 62, 57–65.
- Lu, H.F., Kong, X.X., Huang, H.F., Zhou, Y., Chen, Y.F., 2015. Cu-Mn-Ce ternary mixed-oxide catalysts for catalytic combustion of toluene. *J. Environ. Sci.* 32, 102–107.
- Ma, Y., Chen, M., Song, C., Zheng, X., 2008. Catalytic oxidation of toluene, acetone and ethyl acetate on a new Pt-Pd/Stainless steel wire mesh catalyst. *Acta Phys. Chim. Sin.* 24, 1132–1136.
- Minicò, S., Scirè, S., Crisafulli, C., Maggiore, R., Galvagno, S., 2000. Catalytic combustion of volatile organic compounds on gold/iron oxide catalysts. *Appl. Catal. B Environ.* 28, 245–251.
- Kamal, M.S., Razzak, S.A., Hossain, M.M., 2016. Catalytic oxidation of volatile organic compounds (VOCs) - a review. *Atmos. Environ.* 140, 117–134.
- Pei, W., Liu, Y., Deng, J., Zhang, K., Hou, Z., Zhao, X., et al., 2019. Partially embedding Pt nanoparticles in the skeleton of 3DOM

- Mn<sub>2</sub>O<sub>3</sub>: an effective strategy for enhancing catalytic stability in toluene combustion. *Appl. Catal. B Environ.* 256, 117814.
- Santos, V.P., Pereira, M.F.R., Orfao, J.J.M., Figueiredo, J.L., 2009. Synthesis and characterization of manganese oxide catalysts for the total oxidation of ethyl acetate. *Top. Catal.* 52, 470–481.
- Shu, Y.J., Ji, J., Xu, Y., Deng, J.G., Huang, H.B., He, M., et al., 2018. Promotional role of Mn doping on catalytic oxidation of VOCs over mesoporous TiO<sub>2</sub> under vacuum ultraviolet (VUV) irradiation. *Appl. Catal. B Environ.* 220, 78–87.
- Song, W., Hensen, E.J.M., 2013. A computational DFT study of CO oxidation on a Au nanorod supported on CeO<sub>2</sub>(110): on the role of the support termination. *Catal. Sci. Technol.* 3, 3020–3029.
- Spivey, J.J., 1987. Complete catalytic oxidation of volatile organics. *Ind. Eng. Chem. Res.* 26, 2165–2180.
- Stranick, M.A., 1999. Mn<sub>2</sub>O<sub>3</sub> by XPS. *Surf. Sci. Spectra* 6, 39–46.
- Tang, X., Li, Y., Huang, X., Xu, Y., Zhu, H., Wang, J., et al., 2006. MnO<sub>x</sub>–CeO<sub>2</sub> mixed oxide catalysts for complete oxidation of formaldehyde: effect of preparation method and calcination temperature. *Appl. Catal. B Environ.* 62, 265–273.
- Wang, C., Ma, J., Liu, F., He, H., Zhang, R., 2015. The effects of Mn<sup>2+</sup> precursors on the structure and ozone decomposition activity of cryptomelane-type manganese oxide (OMS-2) catalysts. *J. Phys. Chem. C* 119, 23119–23126.
- Wang, D., Astruc, D., 2017. The recent development of efficient earth-abundant transition-metal nanocatalysts. *Chem. Soc. Rev.* 46, 816–854.
- Wang, F., Dai, H.X., Deng, J.G., Bai, G.M., Ji, K.M., Liu, Y.X., 2012. Manganese oxides with rod-, wire-, tube-, and flower-like morphologies: highly effective catalysts for the removal of toluene. *Environ. Sci. Technol.* 46, 4034–4041.
- Wang, R.H., Li, J.H., 2010. Effects of precursor and sulfation on OMS-2 catalyst for oxidation of ethanol and acetaldehyde at low temperatures. *Environ. Sci. Technol.* 44, 4282–4287.
- Wang, X., 2004. TiO<sub>2</sub> and ZrO<sub>2</sub> crystals in SBA-15 silica: performance of Pt/TiO<sub>2</sub>(ZrO<sub>2</sub>)/SBA-15 catalysts in ethyl acetate combustion. *J. Catal.* 222, 565–571.
- Wang, Y.F., Zhang, C.B., Liu, F.D., He, H., 2013. Well-dispersed palladium supported on ordered mesoporous Co<sub>3</sub>O<sub>4</sub> for catalytic oxidation of o-xylene. *Appl. Catal. B Environ.* 142, 72–79.
- Wu, Z., Jin, R., Wang, H., Liu, Y., 2009. Effect of ceria doping on SO<sub>2</sub> resistance of Mn/TiO<sub>2</sub> for selective catalytic reduction of NO with NH<sub>3</sub> at low temperature. *Catal. Commun.* 10, 935–939.
- Xu, R., Wang, X., Wang, D., Zhou, K., Li, Y., 2006. Surface structure effects in nanocrystal MnO<sub>2</sub> and Ag/MnO<sub>2</sub> catalytic oxidation of CO. *J. Catal.* 237, 426–430.
- Yang, P., Yang, S., Shi, Z., Meng, Z., Zhou, R., 2015. Deep oxidation of chlorinated VOCs over CeO<sub>2</sub>-based transition metal mixed oxide catalysts. *Appl. Catal. B Environ.* 162, 227–235.
- Zhang, J., Li, Y., Wang, L., Zhang, C., He, H., 2015. Catalytic oxidation of formaldehyde over manganese oxides with different crystal structures. *Catal. Sci. Technol.* 5, 2305–2313.
- Zhang, W., Diez-Ramirez, J., Anguita, P., Descorme, C., Valverde, J.L., Giroir-Fendler, A., 2020a. Nanocrystalline Co<sub>3</sub>O<sub>4</sub> catalysts for toluene and propane oxidation: effect of the precipitation agent. *Appl. Catal. B Environ.* 273, 118894.
- Zhang, X., Li, H., Hou, F., Yang, Y., Dong, H., Liu, N., et al., 2017. Synthesis of highly efficient Mn<sub>2</sub>O<sub>3</sub> catalysts for CO oxidation derived from Mn-MIL-100. *Appl. Surf. Sci.* 411, 27–33.
- Zhang, X., Lv, X., Bi, F., Lu, G., Wang, Y., 2020b. Highly efficient Mn<sub>2</sub>O<sub>3</sub> catalysts derived from Mn-MOFs for toluene oxidation: the influence of MOFs precursors. *Mol. Catal.* 482, 110701.
- Zhao, J., Zhao, Z., Li, N., Nan, J., Yu, R., Du, J., 2018. Visible-light-driven photocatalytic degradation of ciprofloxacin by a ternary Mn<sub>2</sub>O<sub>3</sub>/Mn<sub>3</sub>O<sub>4</sub>/MnO<sub>2</sub> valence state heterojunction. *Chem. Eng. J.* 353, 805–813.
- Zhao, Q., Liu, Q., Zheng, Y., Han, R., Song, C., Ji, N., et al., 2020. Enhanced catalytic performance for volatile organic compound oxidation over in-situ growth of MnO<sub>x</sub> on Co<sub>3</sub>O<sub>4</sub> nanowire. *Chemosphere* 244, 125532–125541.
- Zhou, J., Li, Y., Hong, G., Yang, L., Jiang, J., Feng, Y., et al., 2015. Characteristics and health risk assessment of VOCs emitted from pharmaceutical industry of Shijiazhuang city. *Asian J. Ecotox.* 10, 177–186.